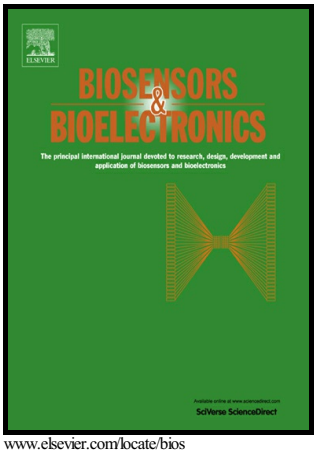

www.elsevier.com/locate/bios

SINGLE-WALLED CARBON NANOTUBES COVALENTLY FUNCTIONALIZED WITH POLYTYROSINE: A NEW MATERIAL FOR THE DEVELOPMENT OF NADH-BASED BIOSENSORS

Marcos Eguílaz, Fabiana Gutierrez, Jose Miguel González-Domínguez, María T. Martínez, Gustavo Rivas

PII: S0956-5663(16)30535-8
DOI: http://dx.doi.org/10.1016/j.bios.2016.06.003
Reference: BIOS8795

To appear in: *Biosensors and Bioelectronic*

Received date: 20 April 2016
Revised date: 1 June 2016
Accepted date: 2 June 2016

Cite this article as: Marcos Eguílaz, Fabiana Gutierrez, Jose Miguel González Domínguez, María T. Martínez and Gustavo Rivas, SINGLE-WALLED CARBON NANOTUBES COVALENTLY FUNCTIONALIZED WITH POLYTYROSINE: A NEW MATERIAL FOR THE DEVELOPMENT OF NADH-BASED BIOSENSORS, *Biosensors and Bioelectronic* http://dx.doi.org/10.1016/j.bios.2016.06.003

SINGLE-WALLED CARBON NANOTUBES COVALENTLY FUNCTIONALIZED WITH POLYTYROSINE: A NEW MATERIAL FOR THE DEVELOPMENT OF NADH-BASED BIOSENSORS

Marcos Eguílaz[1], Fabiana Gutierrez[1], Jose Miguel González-Domínguez[2,3], María T. Martínez[2*], Gustavo Rivas[1,*]

[1]INFIQC. Departamento de Fisicoquímica. Facultad de Ciencias Químicas. Ciudad Universitaria. 5000 Córdoba. Argentina.

[2]Grupo de nanoestructuras de carbono y Nanotecnología. Departamento de Nanotecnología. Instituto de Carboquímica (CSIC). 50018 Zaragoza. Spain.

[3]MSOC-Nanochemistry Group, Faculty of Chemistry, Universidad de Castilla-La Mancha. Avda. Camilo José Cela S/N, 13071, Ciudad Real. Spain.

grivas@fcq.unc.edu.ar

mtmartinez@icb.csic.es

***Corresponding authors: Phone number: +54-351-4334169/80; Fax number: +54-351-4334188.**

Abstract

We report for the first time the use of single-walled carbon nanotubes (SWCNT) covalently functionalized with polytyrosine (Polytyr) (SWCNT-Polytyr) as a new electrode material for the development of nicotinamide adenine

dinucleotide (NADH)-based biosensors. The oxidation of glassy carbon electrodes (GCE) modified with SWCNT-Polytyr at potentials high enough to oxidize the tyrosine residues have allowed the electrooxidation of NADH at low potentials due to the catalytic activity of the quinones generated from the primary oxidation of tyrosine without any additional redox mediator. The amperometric detection of NADH at 0.200 V showed a sensitivity of (217 ± 3) μA mM^{-1} cm^{-2} and a detection limit of 7.9 nM. The excellent electrocatalytic activity of SWCNT-Polytyr towards NADH oxidation has also made possible the development of a sensitive ethanol biosensor through the immobilization of alcohol dehydrogenase (ADH) via Nafion entrapment, with excellent analytical characteristics (sensitivity of (5.8 ± 0.1) μA mM^{-1} cm^{-2}, detection limit of 0.67 μM) and very successful application for the quantification of ethanol in different commercial beverages.

Keywords: Covalently functionalized carbon nanotubes; Polytyrosine; Electrochemical ethanol biosensor; Electrochemical NADH sensor; NADH electrocatalytic oxidation; Alcohol dehydrogenase.

1. Introduction

Dihydronicotinamide adenine dinucleotide (NADH) and its oxidized form nicotinamide adenine dinucleotide (NAD^+) are important coenzymes involved in enzymatic reactions where participate more than 300 dehydrogenases (Li et al., 2014). Electrochemical tecnhiques have been widely used for the quantification of NADH due to their known advantages like high sensitivity, short response time, excellent reproducibility, facile operation and low cost (Radoi and Compagnone, 2009). In fact, NAD^+-dependent electrochemical biosensors have

been focused on the determination of the electrooxidation of NADH (Li et al., 2014; Radoi and Compagnone, 2009; Rassaei et al., 2014). However, in spite of these advantages, the electrochemical quantification of NADH presents some problems connected with the requirement of elevated overvoltages for the direct electrooxidation of NADH, with the consequent effect on the selectivity of the assay (Li et al., 2014), and the passivation of the electrodes produced by the NADH oxidation products, that affects the reproducibility and stability of the platform (Li et al., 2014; Radoi and Compagnone, 2009).

Considerable efforts have been made to decrease the oxidation overvoltage and increase the sensitivity of the electrochemical quantification of NADH. Some redox mediators have been used as shuttle for the electron transport from NADH to the electrode surface (Canevari et al., 2011; Dilgin et al., 2013; Gamella et al. 2010; Lee and Compton, 2013; Mao et al., 2011; Nassef et al., 2006; Prieto-Simon and Fábregas, 2004; Revenga-Parra et al., 2012; Zanardi et al., 2015) reducing, in this way, the energy necessary for NADH oxidation and improving the efficiency of the electrocatalytic oxidation process. The modification of electrodes with carbon nanomaterials (Gasnier et al., 2013; Sun et al., 2013; Wang et al., 2012), nanoparticles (Chen et al., 2013; Jena and Raj, 2006; Sharifi et al., 2013) or hybrid nanomaterials (Agüí et al., 2009; Govindhan et al., 2015; Hosseini et al., 2014; Mundaca et al., 2012; Teymourian et al., 2013; Tiwari and Gupta, 2014) have demonstrated to be highly successful. Polymer-modified electrodes have been also used to incorporate a suitable mediator in the polymer matrix either by covalent or non-covalent immobilization or through physical entrapment in the polymeric matrix (Al-Jawadi et al., 2012; Balamurugan et al., 2010; Gasnier et al., 2012; Hoshino and Muruguma, 2012;

Mota-Ferreira et al., 2013). However, there are just few reports about the electrocatalytic oxidation of NADH at electrodes modified with polymers that works themselves as redox mediators, e.g. poly(3,4)-ethylenedioxytiophene (Rajaram et al., 2015), poly-thionine (Li et al., 2013a), poly-xanthurenic acid (Dos-Santos et al., 2010; Lin et al., 2013), poly-luminol (Lin et al., 2012) or pyrocatechol violet (Zhu et al., 2014).

In this work, we report for the first time: i)the electrocatalytic oxidation of NADH at glassy carbon electrodes (GCEs) modified with a dispersion of single-walled carbon nanotubes (SWCNT) covalently functionalized with polytyrosine (Polytyr); and ii) the application of the resulting GCE/SWCNT-Polytyr to develop a sensitive ethanol biosensor through the incorporation of alcohol dehydrogenase (ADH) via Nafion (Naf) entrapment. To the best of our knowledge, the use of Polytyr as a mediator for the electron transfer in electrochemical experiments has not been reported.

Recently, we have demonstrated the successful functionalization of SWCNT with Polytyr (SWCNT-Polytyr), the efficient dispersion in 50:50 v/v ethanol:water and the robust immobilization at GCE (GCE/SWCNT-Polytyr) (Eguílaz et al., 2016). In the following sections we discuss the electrocatalytic oxidation of NADH, the optimization of the conditions for preparing GCE/SWCNT-Polytyr/ADH/Naf, and the analytical performance of the resulting biosensor.

2. Experimental

2.1. Chemicals and solutions

Single-walled carbon nanotubes (SWCNT, AP-SWNT grade), were supplied from Carbon Solutions Inc. (Riverside, California). ADH (EC. 1.1.1.1, 451 U mg^{-1} solid, from *Saccharomyces cerevisae*), Poly-L-Tyrosine (Polytyr), N,N-diisopropylethylamine (EDIPA), thionyl chloride, β-nicotinamide adenine dinucleotide hydrate (oxidized form, NAD^+), β-nicotinamide adenine dinucleotide reduced disodium salt hydrate (reduced form, NADH) and Nafion perfluorinated solution were purchased from Sigma. Ethanol, ascorbic acid (AA), NaH_2PO_4 and Na_2HPO_4 were obtained from Baker. Methanol and isopropyl alcohol were purchased from Biopack. β-D-(+)-glucose was obtained from Merck. Other chemicals were of analytical grade and used without further purification. Commercial alcoholic beverages were purchased from a local store.

A 0.050 M phosphate buffer solution pH 7.40 was employed as supporting electrolyte. Ultrapure water (ρ = 18.2 MΩ cm) from a Millipore-MilliQ system was used for preparing all aqueous solutions.

2.2. Apparatus

Sonication treatments were carried out with an ultrasonic processor VCX 130W (Sonics and Materials, Inc.), of 20 kHz frequency with a titanium alloy microtip (3 mm diameter). An Allegra™ 21 ultracentrifuge (Beckman Coulter) with a F2402H rotor was used to centrifuge the samples after sonication.

Electrochemical experiments were carried out with TEQ_04 potentiostat using three-electrodes glass electrochemical cells (BAS, Model MF-1084). Bare glassy carbon (GCE, CH Instruments, 3mm diameter) and modified glassy carbon electrodes were used as working electrodes. A platinum wire and Ag/AgCl, 3 M NaCl (BAS, Model RE-5B) were used as auxiliary and reference

electrodes, respectively. All potentials are referred to this reference electrode. A magnetic stirrer under controlled speed provided the convective transport during the amperometric measurements.

2.3. Preparation of SWCNT-Polytyr and their dispersion

SWCNT were CCCfunctionalized as reported elsewhere (Eguílaz et al. 2016). Briefly, this process can be described as: 1) air oxidation of pristine SWCNT at 350ºC for 2h; 2) reflux of air-treated SWCNT in HCl 3M for 2h, resulting in purified SWCNTs; 3) oxidation of purified SWCNTs by reflux in a 3M sulfonitric mixture (H_2SO_4/HNO_3, 50:50 v/v) for 2h, yielding oxidized SWCNT; 4) activation of the carboxylate groups present in the oxidized SWCNT by treatment with thionyl chloride; 5) reaction of the activated oxidized SWCNT with Polytyr.

SWCNT-Polytyr dispersion was prepared according to the protocol previously reported (Eguílaz et al., 2016). Concisely, 1.0 mg of SWCNT functionalized with Polytyr were mixed with 1.0 mL of 50:50 v/v ethanol/water followed by sonication with a sonicator probe for 10.0 min. The amplitude was 50% and the sample was kept in an ice-bath during the procedure. After this treatment, the samples were centrifuged at 9000 rpm for 15 min and the supernatant collected for further work.

2.4. Preparation of GCE modified with SWCNT-Polytyr (GCE/SWCNT-Polytyr)

The GCEs were first polished with alumina slurries of 1.0, 0.3 and 0.05 μm for 1.0 min each, rinsed thoroughly with deionized water, sonicated for 30s in

water, and finally dried under a nitrogen stream. The modification of GCE was performed by casting 20 µL of SWCNT-Polytyr dispersion on the electrode surface and dried at room temperature for 30 min. Before using, GCE/SWCNT-Polytyr was cycled ten times between -0.300 and 0.900 V at 0.100 V s^{-1} in a 0.050 M phosphate buffer solution pH 7.40.

2.5. Construction of the ethanol biosensor

Alcohol dehydrogenase (ADH) was deposited onto the GCE/SWCNT-Polytyr by dropping 20 µL of a 54 units.mL^{-1} ADH solution (prepared in a 0.050 M phosphate buffer solution pH 7.40) onto the modified electrode surface, and dried at room temperature for 60 min. Subsequently, a 5 µL-aliquot of a 0.1% (w/v) Nafion solution (prepared in 0.050 M phosphate buffer solution pH 7.40) was deposited onto the biosensor surface and allowed to dry at room temperature.

2.6. Procedure

The electrochemical experiments were performed in a 0.050 M phosphate buffer solution pH 7.40. Cyclic voltammetry (CV) was carried out in the range between –0.300 V and 0.900 V at a scan rate of 0.100 Vs^{-1}. Amperometric experiments were performed in stirred solutions by applying the desired potential and allowing the transient current to reach a steady-state value prior to the addition of the analyte and the subsequent current monitoring. All experiments were conducted at room temperature.

2.7. Determination of ethanol in alcoholic beverage samples

Commercial alcoholic drinks (white wine, beer and alcoholic mixed drink) were used to evaluate the analytical performance of the proposed biosensor. Stocks solutions were prepared in a 0.050 M phosphate buffer solution pH 7.40. Aliquots of 10 µL of 1:200 white wine stock solution or 10 µL of 1:100 stock solutions in case of beer and mixed alcoholic drink were transferred to the electrochemical cell containing 5.0 mL of NAD^+ $2.0x10^{-3}$ M prepared in a 0.050 M phosphate buffer solution pH 7.40. In all cases the determination of ethanol was performed by amperometry at 0.200 V and the ethanol content was determined by using the standard additions method.

3. RESULTS AND DISCUSSION

3.1 Electrochemical behavior of GCE/SWCNT-Polytyr

Figure 1 shows ten successive cyclic voltammograms obtained at GCE/SWCNT-Polytyr between -0.300 V and 0.900 V in a 0.050 M phosphate buffer solution pH 7.40 at 0.100 Vs^{-1}. In the first cycle there is a peak current at 0.700 V due to the irreversible oxidation of the tyrosine residues (Eguílaz et al., 2016; González-Dominguez et al., 2015; Wang and Bi, 2013a), and a cathodic peak at 0.085 V. In the second cycle a new anodic peak is defined at 0.185V, the peak at 0.700 V largely decreases, while the cathodic peak at 0.085 V remains almost constant. Successive voltammograms show a more clear definition of the quasi-reversible peaks system at 0.185 V/0.085V, attributed to the formation of a quinonoid redox system as secondary products of the oxidation of tyrosine residues (Dos-Santos et al., 2010; Haccoun et al., 2006; Lin et al., 2013; Maleki et al., 2012), and almost the disappearance of the

oxidation current peak at 0.700 V. It is important to mention that voltammograms performed between -0.300 and 0.400 V did not present this peaks system (not shown), demonstrating that it is obtained only if the potential reached in the first cycle is high enough to oxidize the tyrosine residues. Both, anodic and cathodic peak currents present a linear relationship between 0.005 and 0.250 V s^{-1} indicating that the quinone derivatives are originated at the electrode surface giving place to a surface-confined electrochemical process (Inset Fig. 1).

3.2. Electrochemical oxidation of NADH at GCE/MWCNT-Polytyr

Figure 2 displays cyclic voltammograms for $1.0x10^{-3}$ M NADH at different electrodes: GCE (a), GCE/SWCNT-Polytyr (b) and GCE/SWCNT-Polytyr after ten cycles between -0.300 V and 0.900 V at 0.100 Vs^{-1} (defined as GCE/SWCNT-Polytyr(oxidized)) (c). At GCE, NADH is irreversibly oxidized at 0.730 V. When GCE is modified with SWCNT-Polytyr (b), there are two anodic peaks, one at 0.700 V due to the oxidation of tyrosine residues and the other at 0.335 V, corresponding to the oxidation of NADH, demonstrating that SWCNT produces a decrease in the overpotential for the oxidation of NADH of around 400 mV compared to bare GCE. At GCE/SWCNT-Polytyr(oxidized) (c), there is a large anodic peak at 0.200 V. To understand this behavior, is important to analyze the inset of Figure 2, that displays potentiodynamic voltammograms obtained at oxidized GCE/SWCNT-Polytyr in the absence (dashed line) and presence (solid line) of $1.0x10^{-3}$ M NADH. In the absence of NADH, as is expected according to Figure 1, there is a pair of redox peaks attributed to the quinone derivatives generated as secondary products of the oxidation of

tyrosine residues. Upon addition of NADH (solid line), the current of the anodic peak largely increases, as expected for a catalytic process. Therefore, the oxidation of NADH at GCE/SWCNT-Polytyr(oxidized) occurs at potentials even lower than at GCE/SWCNT-Polytyr and significantly lower than at bare GCE (530 mV), demonstrating that the quinone derivatives present at the surface of GCE/SWCNT-Polytyr(oxidized), largely catalyzes the electrooxidation of NADH

Figure 3A displays the amperometric response obtained at 0.200 V at GCE/SWCNT-Polytyr(oxidized) for successive additions of NADH. A clearly defined and fast response is observed after each addition of NADH with steady-state currents reached in 5 s. The calibration plot (Figure 3B) demonstrates a wide linear range from $1.5x10^{-7}$ M to $8.3x10^{-5}$ M, with a sensitivity of (217 ± 3) μA mM cm^{-2}, (r^2=0.995), and a detection limit of $7.9x10^{-9}$ M (taken as 3.3 σ/S, where σ is the standard deviation of the blank signal and S, the sensitivity). The sensitivities obtained from the amperometric response to NADH using five different GCE/SWCNT-Polytyr(oxidized) gave a RSD value of 2.5%.

The analytical performance of GCE/SWCNT-Polytyr(oxidized) was compared to that of other NADH sensors reported in the last years (Table 1). The wide linear range of the proposed sensor (that covers almost three orders of magnitude), the sensitivity and detection limit of the proposed NADH sensor are better than most of those showed in Table 1. NADH sensors based on hybrid materials of ordered carbohydrate derived porous carbons/gold nanoparticles (Hosseini et al., 2014) and reduced graphene oxide/gold nanoparticles (Govindhan et al., 2015) showed better sensitivities and lower detection limits, however, the operating potentials are higher than the one used

in this work. In addition, our NADH sensor exhibits the important advantage of avoiding the use of external redox mediators.

Figure 3C compares the amperometric response of $1.0x10^{-4}$ M NADH over a continuous 25 min period at bare GCE (a) and at GCE/SWCNT-Polytyr(oxidized) (b) held at 0.400 V. The bare GCE displays a rapid decay of the signal (there is a decrease of 50.1%, 59.4% and 72.6% after 5, 10 and 25 min, respectively), indicating a great inhibition of the electron transfer process. In contrast, the response at GCE/SWCNT-Polytyr(oxidized) remains stable throughout the entire experiment, with only 2.4%, 3.6% and 8.2% current decreases at 5, 10 and 25 min, respectively, demonstrating an important resistance of the GCE/SWCNT-Polytyr to the fouling due to NADH oxidation. This attractive feature makes possible an excellent reusability, with a RSD of 5.8% for eight successive calibrations at 0.200 V using the same electrode surface.

3.3 Electrochemical biosensing of ethanol at GCE/SWCNT-Polytyr/ADH/Naf

GCE/SWCNT-Polytyr(oxidized) was used as a new platform for the construction of a very simple ethanol biosensor based on the immobilization of ADH at GCE/SWCNT-Polytyr through entrapment with Nafion (to allow a robust immobilization) using NAD^+ as cofactor. The analytical signal of the amperometric biosensor was obtained from the oxidation of NADH enzymatically generated by ADH in the presence of NAD^+.

The amount of immobilized ADH and concentration of NAD^+ are very important parameters in the development of the biosensor. Figure 4A shows the sensitivities of ethanol obtained at 0.200 V in a 0.050 phosphate buffer solution

pH 7.40 containing $2.0x10^{-3}$ M NAD^+ for different biosensors prepared with various ADH loadings ranging from 0.27 to 2.16 units. The sensitivity increases with the amount of ADH up to 1.08 units, and remains almost constant for higher enzyme loadings. Accordingly, 1.08 units of ADH were selected as enzyme loading for the biosensor preparation.

Since NAD^+ plays a key role as acceptor of the electrons generated in the enzymatic reaction, we evaluated the effect of NAD^+ concentration on the sensitivity of GCE/SWCNT-Polytyr(oxidized)/ADH/Naf biosensor to ethanol in the presence of different concentrations of NAD^+ from $5.0x10^{-4}$ to $5.0x10^{-3}$ M. Figure 4B shows a sharp rise in the sensitivity up to $2.0x10^{-3}$ M NAD^+, with a slight decrease for higher concentrations, attributed to a slight inhibitory effect observed for higher concentrations of NAD^+ (Agüí et al., 2009). Therefore, $2.0x10^{-3}$ M NAD^+ in solution was selected to establish the analytical characteristics of the developed biosensor.

Figure 5 displays the amperometric response obtained at GCE/SWCNT-Polytyr(oxidized)/ADH/Naf at 0.200 V for successive additions of ethanol into a stirred 0.050 M phosphate buffer solution pH 7.40 containing $2.0x10^{-3}$ M NAD^+ (A) and the corresponding calibration curve (B). A well-defined response is obtained after the addition of ethanol, with steady-state values reached within 15 s. A linear response of the biosensor was obtained between $1.0x10^{-5}$ and $1.5x10^{-4}$ M (r^2=0.9991), with a sensitivity of (1.56 ± 0.03) μA mM^{-1} or (5.8 ± 0.1) μA mM^{-1} cm^{-2}). The limit of detection was 0.67 μM (calculated as it was previously indicated). Table 2 compares the analytical performance of GCE/SWCNTs-Polytyr(oxidized)/ADH/Naf biosensor with those of other ADH-based biosensors. Our biosensor represents a very competitive alternative

since the sensitivity and detection limit are better than most of the reported ADH-based biosensors. Ethanol biosensors based on graphene/gold nanorods (Li et al., 2013b) and diphenylalanine peptide/carbon nanotube composite (Yuan et al., 2011) showed better sensitivities, although the operating potentials are higher than the one used in this work. Moreover, the detection limit obtained with our biosensor is lower than most of the ones reported in Table 2. In fact, our detection limits are lower than that that reported for biosensors based on non-covalently functionalized carbon nanotubes with 1,10-phenanthroline-5,6-dione (300 µM) (Mao et al., 2011), diphenylalanine peptide/carbon nanotube composite (12 µM) (Yuan et al., 2011), nickel oxide nanoparticles (6.4 µM) (Sharifi et al., 2013), reduced graphene oxide functionalized with polydopamine and gold nanoparticles (88 µM) (Tian et al., 2013), screen-printed electrodes modified with a graphitized mesoporous carbon/chitosan/meldola`s blue/NAD^+ nanobiocomposite (80 µM) (Hua et al., 2013), platinum nanoparticles/dendritic hyperbranched carboxilane polymer nanobiocomposite (451.6 µM) (Jiménez et al., 2014); and comparable to that obtained for electrogenerated NAD^+ oxidation product immobilized onto carbon nanotubes/ionic liquid nanocomposite (0.5 µM) (Teymourian et al., 2012a), electroreduced graphene oxide-polythionine composite (0.3 µM) (Li et al., 2013a), poly(3,4-ethylenedioxythiophene)/gold nanoparticles (2 µM) (Serafin et al., 2011) and graphene/gold nanorods (1.5 µM) (Li et al., 2013b).

The sensitivities obtained with five different GCE/SWCNT-Polytyr(oxidized)/ADH/Naf biosensors gave a RSD of 2.9%, indicating a good reproducibility in the overall fabrication process. No interference was observed after additions of methanol, isopropyl alcohol and glucose (not shown).

The GCE/SWCNT-Polytyr(oxidized)/ADH/Naf biosensor was used to quantify the content of ethanol in commercial alcoholic drinks. The concentrations of ethanol in the different beverages are the following: beer 1 (5.0 ± 0.1) %v/v, beer 2 (4.9 ± 0.1) %v/v, mixed drink (6.6 ± 0.2) %v/v, and white wine (13.6 ± 0.2) %v/v, demonstrating an excellent correlation with the values reported by the suppliers (4.9, 5.0, 6.5, and 13.5 % v/v, respectively). Therefore, the proposed biosensor clearly demonstrate the analytical usefulness of the proposed electrochemical biosensor to determine the ethanol content in real samples.

CONCLUSIONS

The results presented here have allowed us to demonstrate that the covalent functionalization of SWCNT with Polytyr not only makes possible an efficient dispersion of the nanostructures but also facilitates the electrooxidation of NADH through the catalytic activity of the products of tyrosine primary oxidation. The GCE/SWCNT-Polytyr(oxidized) represents a new and advantageous alternative for the highly sensitive electrochemical sensing of NADH and a robust bioanalytical platform for the construction of an enzymatic ethanol biosensor based on ADH/NAD^+ without the need of redox mediators and excellent analytical performance in real samples.

Acknowledgements

The authors thank Spanish MINECO (PRI-PIBAR-2011-1), the Government of Aragon (Project DGA-ESF-T66 CNN), the European Social Fund (ESF),

CONICET, SECyT-UNC, MINCyT-Córdoba, ANPCyT and PICT MICINN 2011-2748) for the financial support. M.E. acknowledge CONICET for the fellowship.

REFERENCES

Agüí, L., Eguílaz, M., Peña-Farfal, C. Yáñez-Sedeño, P., Pingarrón, J.M., 2009. Electroanalysis 21, 386-391.

Al-Jawadi, E., Poller, S., Haddad, R., Schuhmann, W., 2012. Microchim. Acta 177, 405-410.

Balamurugan, A., Ho, K.C., Chen, S.M., Huang, T.Y., 2010. Colloid Surface A 362, 1-7.

Canevari, T.C., Vinhas, R.C.G., Landers, R., Gushikem, Y., 2011. Biosens. Bioelectron. 26, 2402-2406.

Chen, C.H., Chen, Y.C., Lin, M.S., 2013. Biosens. Bioelectron. 42, 379-384.

Dilgin, Y., Kizilkaya, B., Dilgin, D.G., Gökçel, H.I., Gorton, L., 2013. Colloid Surface B 102, 816-821.

Dos Santos-Silva, F.,Bezerra-Lopes, C., de Oliveira-Costa, E., Rodrigues-Lima, P., Tatsuo-Kubota, L., Fonseca-Goulart, M.O., 2010. Electrochem. Commun. 12, 450-454.

Eguílaz, M., Guitérrez, A., Gutiérrez, F., González-Domínguez, J.M., Ansón-Casaos, A., Hernández-Ferrer, J., Ferreyra, N.F., Martínez, M.T., Rivas, G., 2016. Anal. Chim. Acta 909, 51-59.

Fan, Y., Yang, X., Yang, C., Liu, J., 2012. Electroanalysis 6, 1334-1339.

Gasnier, A., Pedano, M.L., Gutierrez, F., Labbe, P., Rivas, G.A., 2012. Electrochim. Acta 71, 73-81.

Gasnier, A., Pedano, M.L., Rubianes, M.D., Rivas, G.A., 2013. Sens. Actuators, B 176, 921-926.

Ge, B., Tan, Y., Xie, Q., Ma, M., Yao, S., 2009. Sens. Actuators, B 137, 547-554.

González-Domínguez, J.M., Gutierrez, F.A., Hernández-Ferrer, J., Ansón-Casaos, A., Rubianes, M.D., Rivas, G., Martínez, M.T., 2015. J. Mat. Chem. B 3, 3870-3884.

Gamella, M., Campuzano, S., Conzuelo, F., Curiel, J.A., Muñoz, R., Reviejo, A.J., Pingarrón, J.M., 2010. Talanta 81, 925-933.

Govindhan, M., Amiri, M., Chen, A., 2015. Biosens. Bioelectron. 66, 474-480.

Haccoun, J., Piro, B., Nöel, V., Pham, M.C., 2006. Bioelectrochemistry 68, 218-226.

Hoshino. T., Muruguma, H., 2012. Electrochemistry 80, 85-87.

Hosseini, H., Behbahani, M., Mahyari, M., Kazerooni, H., Bagheri, A., Shaabani, A., 2014. Biosens. Bioelectron. 59, 412-417.

Hua, E., Wang, L., Jing, X., Chen, C., Xie, G., 2013. Talanta 111, 163-169.

Huang, T.Y., Huang, J.H., Wei, H.Y., Ho, K.C., Chu, C.W., 2013. Biosens. Bioelectron. 43, 173-179.

Jena, B.K., Raj, C.R., 2006. Anal. Chem. 78, 6332-6339.

Jiménez, A., García-Armada, M.P., Losada, J., Villena, C., Alonso, B., Casado, C.M., 2014. Sens. Actuators, B 190, 111-119.

Keeley, G.P., O´Neill, A., Holzinger, M., Cosnier, S., Coleman, J.N., Duesberg, G.S., 2011. Phys. Chem. Chem. Phys. 13, 7747-7750.

Lee, P.T., Compton, R.G., 2013. Electroanalysis 25, 1613-1620.

Li, Z., Huang, Y., Chen, L., Qin, X., Huang, Z., Zhou, Y., Meng, Y., Li, J., Huang, S., Liu, Yan, Wang, W., Xie, Q., Yao, S., 2013a. Sens. Actuators, B 181, 280-287.

Li, L., Lu, H., Deng, L., 2013b. Talanta 113, 1-6.

Li, Y.W., Chen, Y. Ma, Y.H., Shi, J.G., Wang, Y.X., Qi, C.H., Li, Q.S., 2014. Chin. J. Anal. Chem. 42(5), 759–765.

Lin, K.C., Yin, C.Y., Chen, S.M., 2012. Analyst 137, 1378-1383.

Lin, K.C., Li, Y.S., Chen, S.M., 2013. Sens. Actuators, B 184, 212-219.

Maleki, A., Nematollahi, D., Clausmeyer, J., Henig, J., Plumeré, N., Wolfgang, S., 2012. Electroanalysis 24, 1932-1936.

Mao, X., Wu, Y., Xu, L., Cao, X., Cui, X., Zhu, L., 2011. Analyst 136, 293-298.

Mota-Ferreira, G.M., Mota-de Oliveira, F., Figueiredo-Leite, F.R., Maroneze, C.M., Kubota, L.T., Damos, F.S., Silva-Luz, R.C., 2013. Electrochim. Acta 111, 543-551.

Mundaca, R.A., Moreno-Guzmán, M., Eguílaz, M., Yáñez-Sedeño, P., Pingarrón, J.M., 2012. Talanta 99, 607-702.

Nassef, H.M., Radi, A.E., O´Sullivan, C.K., 2006. Electrochem. Commun. 8, 1719-1725.

Prieto-Simon, B., Fábregas, E., 2004. Biosens. Bioelectron. 19, 1131-1138.

Radoi, A., Compagnone, D., 2009. Bioelectrochemistry 76, 126-134.

Rajaram, R., Anandhakumar, S., Mathiyarasu, J., 2015. J. Electroanal. Chem. 746, 75-81.

Rassaei, L., Olthuis, W., Tsujimura, S., Sudholter, E.J.R., van den Berg, A., 2014. Anal. Bioanal. Chem. 406, 123-137.

Revenga-Parra, M., Gomez-Anquela, C., Garcia-Mendiola, T., Gonzalez, E., Pariente, F., Lorenzo, E., 2012. Anal. Chim. Acta 747, 84-91.

Rotariu, L., Istrate, O.M., Bala, C., 2014. Sens. Actuators, B 191, 491-497.

Saleh, F.S., Okajima, T., Kitamura, F., Mao, L., Ohsaka, T., 2011. Electrochim. Acta 56, 4916-4923.

Serafin, V., Agüí, L., Yañez-Sedeño, P., Pingarrón, J.M., 2011. J. Electroanal. Chem. 656, 152-158.

Sharifi, E., Salimi, A., Shams, A., 2013. Biosens. Bioelectron. 45, 260-266.

Sun, Y., Ren, Q., Liu, X., Zhao, S., Qin Y., 2013. Biosens. Bioelectron. 39, 289-295.

Teymourian, H., Salimi, A., Hallaj, R., 2012a. Talanta 90, 91-98.

Teymourian, H., Salimi, A., Hallaj, R., 2012b. Biosens. Bioelectron. 33, 60-68.

Teymourian, H., Salimi, A., Khezrian, S., 2013. Biosens. Bioelectron. 49, 1-8.

Tian, J., Deng, S.Y., Li, D.L., Shan, D., He, W., Zhang, X.J., Shi, Y., 2013. Biosens. Bioelectron. 49, 466-471.

Tiwari, I., Gupta, M., 2014. Mater. Res. Bull. 49, 94-101.

Wang, Z., Shoji, M., Hironori, O., 2012. Talanta 99, 487-491.

Wang, Y., Bi, C., 2013a. J. Mol. Liq. 177, 26-31.

Wang, Z., Etienne, M., Urbanova, V., Kohring, G.W., Walcarius, A. 2013b. Anal. Bioanal. Chem. 405, 3899-3906.

You, J.M., Jeon, S., 2011. Electrochim. Acta 56, 10077-10082.

Yuan, J., Chen, J., Wu, X., Fang, K., Niu, L., 2011. J. Electroanal. Chem. 656, 120-124.

Zanardi, C., Ferrari, E., Pigani, L., Arduini, F., Seeber, R., 2015. Chemosensors 3, 118-128.

Zhu, J., Wu, X.Y., Shan, D., Yuan, P.X., Zhang, X.J., 2014. Talanta 130, 96-102.

LEGENDS OF THE FIGURES

Figure 1: Consecutive cyclic voltammograms (10 cycles) obtained at GCE/SWCNT-Polytyr in a 0.050 M phosphate buffer solution pH 7.40. Scan rate:0.100 Vs^{-1}. Inset: Dependence of peak currents on the scan rates.

Figure 2: Cyclic voltammograms obtained for $1.0x10^{-3}$ M NADH at GCE (a), GCE/SWCNT-Polytyr (b) and GCE/SWCNT-Polytyr(oxidized) (c). Inset: Cyclic voltammograms obtained in a 0.050 M phosphate buffer solution pH 7.40 in absence (dashed line) and presence (solid line) of $1.0x10^{-3}$ M NADH at GCE/SWCNT-Polytyr(oxidized). Scan rate: 0.100 Vs^{-1}.

Figure 3: (A) Amperometric recording for successive additions of NADH at GCE/SWCNT-Polytyr(oxidized). a, b, c, d and e correspond to the following concentrations: 7.3×10^{-7} M, 4.2×10^{-6} M, 1.1×10^{-5} M, 2.5×10^{-5} M and 5.7×10^{-5} M. Working potential: 0.200 V. (B) Calibration plot obtained from the amperometric recording shown in Figure 3A. (C) Amperometric recordings for $1.0x10^{-4}$ M NADH at 0.400 V obtained at bare GCE (a) and GCE/SWCNT-Polytyr(oxidized) (b).

Figure 4: (A) Sensitivity for ethanol obtained from amperometric experiments at GCE/SWCNT-Polytyr(oxidized)/ADH/Naf biosensor as a function of the enzyme

units; NAD^+ concentration: $2.0x10^{-3}$ M. (B) Sensitivity towards NADH obtained from amperometric experiments at GCE/SWCNT-Polytyr(oxidized)/ADH/Naf biosensor as a function of the NAD^+ concentration; enzyme units: 1.08 U. Other conditions: supporting electrolyte 0.050 M phosphate buffer solution pH 7.40; working potential: 0.200 V.

Figure 5: (A) Amperometric recording for successive additions of ethanol at GCE/SWCNT-Polytyr(oxidized)/ADH/Naf. a and b correspond to $5.0x10^{-5}$ M and $1.5x10^{-4}$ M ethanol. Working potential: 0.200 V. (B) Calibration plot obtained from the amperometric recording shown in Figure 5A.

Table 1: Comparison of the analytical characteristics of the reported sensor (GCE/SWCNT-Polytyr(oxidized)) with those reported for other NADH sensors.

Electrode	*Technique*	*Sensitivity, μA mM^{-1}*	*Linear range, M*	*LOD, μM*	*Ref.*
SPCE/Azure A	Amp. (0.000 V)	-	$6.6 x10^{-7} – 6.25 x10^{-6}$	0.12	Revenga-Parra et al. (2012)
PGE/QH_2	Amp. (0.300 V)	34	$5.0 x10^{-7} – 1.0 x10^{-4}$	0.15	Dilgin et al. (2013)
CPE-SiO_2/SnO_2/Sb_2O_5/MB	Amp. (-0.050 V)	8.1	$8.0 x10^{-5} – 9.0 x10^{-4}$	0.15	Canevari et al. (2011)
GCE/MWCNTs/PD	Amp. (0.000 V)	8.77	$5.0 x10^{-5} – 5.0 x10^{-4}$	1.8	Mao et al. (2011)
GCE/CNSs	LSV (0.336 V)	85.8 (715 μA mM^{-1} cm^{-2})	$0 – 5.0 x10^{-4}$	0.44	Wang et al. (2012)
GCE/PAA/(CMWCNTs/AMWCNTs)$_4$	Amp. (0.150 V)	(223.8 μA mM^{-1} cm^{-2})	$2.0 x10^{-6} – 1.2 x10^{-3}$	1.5	Sun et al. (2013)
GrPE	DPV (0.350 V)	6.7 ± 0.5	$1.0 x10^{-5} – 2.0 x10^{-4}$	-	Gasnier et al. (2013)
GCE/NiONPs	Amp. (0.350 V)	52	$1.1 x10^{-7} – 1.0 x10^{-3}$	0.106	Sharifi et al. (2013)
RDCE/nCo_3O_4	Amp. (0.100 V)	2.8	$1.0 x10^{-5} - 1.0 x10^{-4}$	4.25	Chen et al. (2013)
GCE/rGO-Fe_3O_4	Amp. (0.050 V)	(113 μA mM^{-1} cm^{-2})	$2.0 x10^{-6} – 1.5 x10^{-5}$	0.40	Teymourian et al. (2013)
GCE/MWCNTs-NR-AuNPs	DPV (0.520 V)	0.588	$1.8 x10^{-5} – 1.4 x10^{-3}$	0.5	Tiwari and Gupta

					(2014)
GCE/OC-DPCs-AuNPs	DPV (0.900 V)	4934	$5.0 \times 10^{-9} – 1.0 \times 10^{-5}$	0.001	Hosseini et al. (2014)
GCE/MWCNTs-PEI-Do	Amp. (-0.025 V)	19	$1.0 \times 10^{-5} – 1.0 \times 10^{-4}$	3	Gasnier et al. (2012)
GCE/rGO-DNA-MB	Amp. (0.100 V)	12.75	$1.0 \times 10^{-5} – 1.5 \times 10^{-3}$	1	Mota-Ferreira et al. (2013)
GCE/$PEDOT_{SDS}$/AgNPs/MB	Amp. (-0.050 V)	2	$1.0 \times 10^{-5} – 5.6 \times 10^{-4}$	0.1	Balamurugan et al. (2010)
GCE/nPEDOT	Amp. (0.500 V)	26	$5.0 \times 10^{-6} – 4.5 \times 10^{-5}$	3.8	Rajaram et al. (2015)
GCE/ERGO-PTH	Amp. (0.400 V)	(143 μA mM^{-1} cm^{-2})	$1.0 \times 10^{-5} – 3.9 \times 10^{-3}$	0.1	Li et al. (2013a)
GCE/MWCNTs-polyXa	Amp. (0.100 V)	(2200 μA mM^{-1} cm^{-2})	$5.0 \times 10^{-7} – 1.0 \times 10^{-5}$	0.1	Dos Santos-Silva et al. (2010)
GCE/CNTs/polyXa-FAD	Amp. (0.150 V)	(155 μA mM^{-1} cm^{-2})	$5.0 \times 10^{-6} – 1.7 \times 10^{-4}$	1	Lin et al. (2013)
GCE/polyLu/MWCNTs	Amp. (0.100 V)	(183.9 μA mM^{-1} cm^{-2})	$5.0 \times 10^{-6} – 1.0 \times 10^{-4}$	0.6	Lin et al. (2012)
PGE/SWCNTs/PCV	Amp. (0.200 V)	(146.2 μA mM^{-1} cm^{-2})	$1.3 \times 10^{-6} – 2.8 \times 10^{-4}$	1.3	Zhu et al. (2014)
SPE/PAH	Amp. (0.600 V)	(126 ± 3 μA mM^{-1} cm^{-2})	$1.0 \times 10^{-5} – 2.0 \times 10^{-4}$	0.22	Rotariu et al. (2014)
GCE/Gr	Amp. (0.400 V)	19.7	$4.5 \times 10^{-5} – 3.6 \times 10^{-4}$	1.9	Keeley et al. (2011)
GCE/AuNPs-TiO_2NPs-Gr	Amp. (0.400 V)	18 (228.7 μA mM^{-1} cm^{-2})	$1.0 \times 10^{-5} – 2.4 \times 10^{-4}$	0.2	Fan et al. (2012)
GCE/MWCNTs-PP	Amp. (0.600 V)	(40.37 μA mM^{-1} cm^{-2})	$2.0 \times 10^{-5} – 8 \times 10^{-4}$	10	Yuan et al. (2011)
EPPG/SWCNTs/PPS	Amp. (0.000 V)	(576 μA mM^{-1} cm^{-2})	1.0×10^{-5} - 1.7×10^{-4}	0.01	Saleh et al. (2011)
GCE/MWCNTs/PMG	Amp. (0.200 V)	-	-	-	Wang et al. (2013b)
AuE/MWCNTs-CS-Do	Amp. (0.250 V)	9.93	$1.0 \times 10^{-7} – 6.0 \times 10^{-4}$	0.012	Ge et al. (2009)
GCE/MWCNTs-IL-OxP(NAD^+)	Amp. (0.100 V)	(440 μA mM^{-1} cm^{-2})	$2.0 \times 10^{-7} – 2.0 \times 10^{-5}$	0.02	Teymourian et al. (2012a)
GCE/MWCNTs-Fe_3O_4NPs	Amp. (0.000 V)	(70 μA mM^{-1} cm^{-2})	$1.0 \times 10^{-6} – 7.0 \times 10^{-5}$	0.3	Teymourian et al. (2012b)
GCE/MWCNTs-PdNPs/PEDOP	Amp. (0.420 V)	12.72	$1.0 \times 10^{-6} – 1.3 \times 10^{-2}$	0.18	You and Jeon (2011)
GCE/SWCNTs-rGO	Amp. (0.100 V)	(204 μA mM^{-1} cm^{-2})	$2.0 \times 10^{-5} – 4.0 \times 10^{-4}$	0.078	Huang et al. (2013)
GCE/Gr-AuNRs	Amp. (0.400 V)	(10.27 μA mM^{-1} cm^{-2})	$2.0 \times 10^{-5} – 1.6 \times 10^{-4}$	6	Li et al. (2013b)
GCE/rGO-AuNPs	Amp. (0.550 V)	(916 μA mM^{-1} cm^{-2})	$5.0 \times 10^{-8} – 5.0 \times 10^{-5}$	0.00113	Govindhan et al. (2015)
GCE/PDRGO-AuNPs	Amp. (0.100 V)	2.82	$5.0 \times 10^{-8} – 4.2 \times 10^{-5}$	-	Tian et al. (2013)
PtE/PtNPs/PDAMS	Amp. (0.500 V)	(68.24 μA mM^{-1} cm^{-2})	$8.7 \times 10^{-5} – 7.0 \times 10^{-4}$	4.78	Jiménez et al. (2014)
SPCE/MB-GMCs-CS	Amp. (-0.150 V)	10.36	$1.0 \times 10^{-5} – 4.1 \times 10^{-4}$	0.186	Hua et al. (2013)
GCE/SWCNTs(oxidized)-Polytyr	Amp. (0.200 V)	68 ± 1 (217 ± 3 μA mM^{-1} cm^{-2})	$1.5 \times 10^{-7} – 8.3 \times 10^{-5}$	0.0079	This work

AgNPs: silver nanoparticles; Amp.: amperometry; aMWCNTs: aminated multi-walled carbon nanotubes; AuE: gold electrode; AuNPs: gold nanoparticles; AuNRs: gold nanorods; cMWCNTs: carboxylated multi-walled carbon nanotubes; CNSs: carbon nanosheets; CPE: carbon paste electrode; CS: chitosan; Do: dopamine; DPV: Differential pulse voltammetry; EPPG: edge-plane pyrolytic graphite; ERGO: electroreduced grephene oxide; Fe_3O_4NPs: magnetite nanoparticles; GCE: glassy carbon electrode; GMCs: graphitized mesoporous carbons; Gr: graphene; IL: ionic liquid; LSV: Linera sweep voltammetry; MB: Meldola´s blue; MeB: methylene blue; MWCNTs: multi-walled carbon nanotubes; nCo_3O_4: cobalt oxide nanosheet; NiONPs: nickel oxide nanoparticles; nPEDOT: nanoporous poly(3,4-ethylene dioxythiophene); NR: neutral red; OC-DPCs: ordered carbohydrate-derived porous carbons; OxP(NAD^+): electrogenerated NAD^+ oxidation products; PAA: poly(allylamine); PAH: poly(allylamine hydrochloride); PCV: pyrocatechol violet; PD: 1,10-phenanthroline-5,6-dione; PDAMS: poly(diallylmethylsilane); PdNPs: palladium nanoparticles; PDRGO: poly(dopamine)-reduced graphene oxide; PEDOP: poly(3,4-ethylene dioxypyrrole); $PEDOT_{SDS}$: poly(3,4-ethylene dioxythiophene-sodium dodecyel sulfate); PEI: poly(ethylenimine); PGE: pencil graphite electrode; PMG: poly(methylene green); polyLu: poly(luminol); polyXa: poly(xanthurenic acid); PP: diphenylalanine peptide; PPS: poly(phenosafranin); PtE: platinum electrode; PTH: poly(thionine); QH_2: quercetin RDCE: rotating disc carbon electrode; rGO: reduced graphene oxide; SCPE: screen-printed carbon electrode; SWCNTs: single-walled carbon nanotubes; TiO_2NPs: titanium oxide nanoparticles.

Table 2: Comparison of the analytical characteristics of the reported biosensor (GCE/SWCNT-Polytyr(oxidized)/ADH/Naf) with those reported for other ADH-based ethanol biosensors.

Electrode	***Technique***	***Sensitivity, μA mM^{-1}***	***Linear range, M***	***LOD, μM***	***Ref.***
PtE/PtNPs/PDAMS/ADH-BSA-GA	Amp. (0.250 V)	(0.233 μA mM^{-1} cm^{-2})	$9.0 \times 10^{-4} – 7.0 \times 10^{-3}$	451.6	Jiménez et al. (2014)
GCE/MWCNTs/PD/ADH/Naf	Amp. (0.000 V)	0.01085	$1.0 \times 10^{-3} – 7.0 \times 10^{-3}$	300	Mao et al. (2011)

GCE/MWCNTs-PP/ADH-BSA-GA	Amp. (0.600 V)	(30 μA mM^{-1} cm^{-2})	3.0 $x10^{-5}$ – 7.0 $x10^{-4}$	12	Yuan et al. (2011)
PGE/SWCNTs/PCV/ADH-BSA-GA	Amp. (0.200 V)	(1.94 μA mM^{-1} cm^{-2})	9.3 $x10^{-6}$ – 3.2 $x10^{-4}$	-	Zhu et al. (2014)
GCE/MWCNTs-IL-OxP(NAD^+)/ADH	Amp. (0.100 V)	1.7	5.0 $x10^{-6}$ – 6.0 $x10^{-5}$	0.5	Teymourian et al. (2012a)
GCE/ERGO-PTH/ADH-BSA-GA	Amp. (0.400 V)	(2.8 μA mM^{-1} cm^{-2})	5.0 $x10^{-5}$ – 1.0 $x10^{-3}$	0.3	Li et al. (2013a)
GCE/PDRGO-AuNPs/NAD^+-ADH-CS	Amp. (0.300 V)	(0.0786 μA mM^{-1} cm^{-2})	up to 3.0 x 10^{-3}	88	Tian et al. (2013)
GCE/Gr-AuNRs/ADH	Amp. (0.400 V)	(102 μA mM^{-1} cm^{-2})	5.0 $x10^{-6}$ – 2.8 $x10^{-4}$	1.5	Li et al. (2013b)
SPCE/AuNPs/PEDOT/ADH	Amp. (0.300 V)	0.727	5.0 $x10^{-6}$ – 1.0 $x10^{-4}$	2	Serafin et al. (2011)
SPCE/MB-GMCs-NAD^+-ADH-CS	Amp. (-0.150 V)	0.06728	5.0 $x10^{-4}$ – 15.0 $x10^{-3}$	80	Hua et al. (2013)
GCE/NiONPs/ADH-Naf	Amp. (0.450 V)	0.036	6.4 $x10^{-6}$ – 6.0 $x10^{-3}$	6.4	Sharifi et al. (2013)
GCE/SWCNTs-Polytyr(oxidized)/ADH/Naf	Amp. (0.200 V)	1.56 ± 0.03 (5.8 ± 0.1 μA mM^{-1} cm^{-2})	1.0 x 10^{-5} – 1.5 x 10^{-4}	0.67	This work

ADH: alcohol dehydrogenase; Amp.: amperometry; AuNPs: gold nanoparticles; AuNRs: gold nanorods; BSA: bovine serum albumin; CS: chitosan; GA: glutaraldehyde; ERGO: electroreduced graphene oxide; GCE: glassy carbon electrode; GMCs: graphitized mesoporous carbons; Gr: graphene; IL: ionic liquid; MB: Meldola blue; MWCNTs: multi-walled carbon nanotubes; NiONPs: nickel oxide nanoparticles; OxP(NAD^+): electrogenerated NAD^+ oxidation products; Naf: nafion; PCV: pyrocatechol violet; PD: 1,10-phenanthroline-5,6-dione; PDAMS: poly(diallylmethylsilane); PDRGO: poly(dopamine)-reduced graphene oxide; PEDOT: poly(3,4-ethylenedioxythiophene); PGE: pencil graphite electrode; PP: diphenylalanine peptide; PtE: platinum electrode; PTH: poly(thionine); PtNPs: platinum nanoparticles; SPCE: screen-printed carbon electrode; SWCNTs: single-walled carbon nanotubes.

Highlights

- The oxidation of SWCNT-Polytyr generates surface quinone groups that facilitates the oxidation of NADH.
- NADH is catalytically oxidized at GCE/SWCNT-$Polytyr_{(oxidized)}$.
- GCE/SWCNT-$Polytyr_{(oxidized)}$ is a robust platform for further immobilization of ADH.
- GCE/SWCNT-$Polytyr_{(oxidized)}$//ADH/Naf allows the quantification of ethanol in alcoholic beverages

FIGURE 1-RIVAS ET AL.

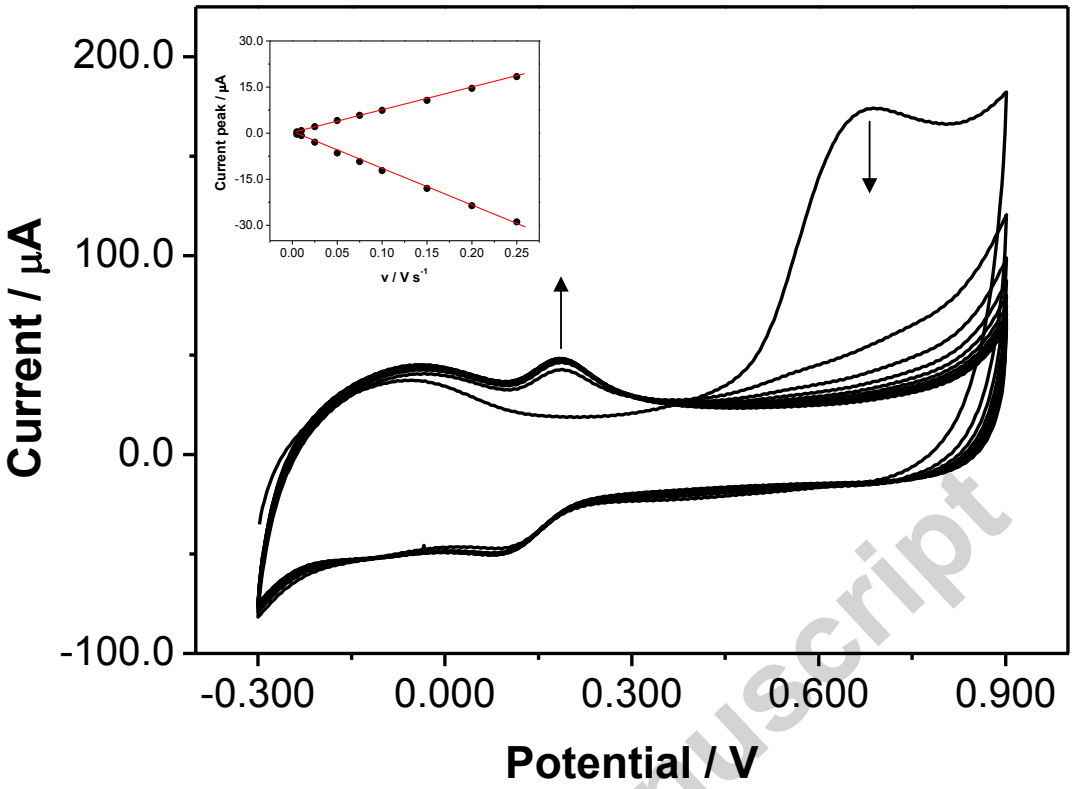

FIGURE 2- RIVAS ET AL.

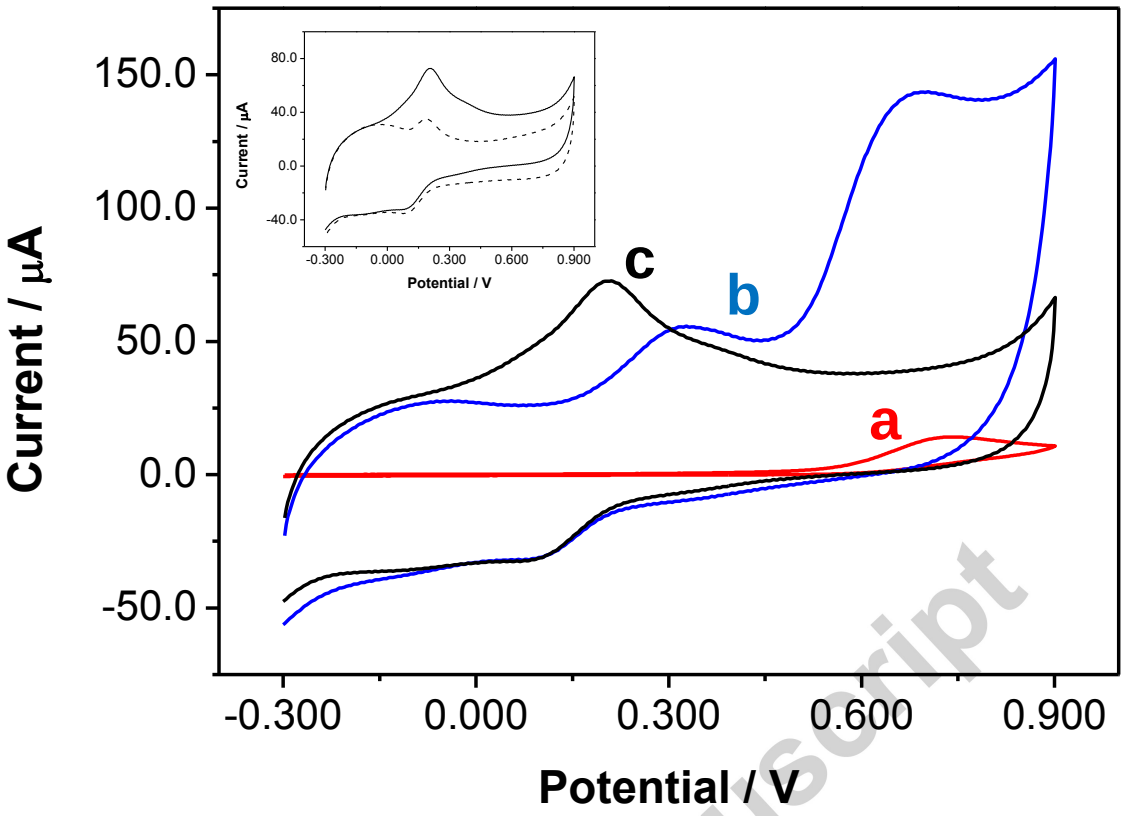

FIGURE 3- RIVAS ET AL.

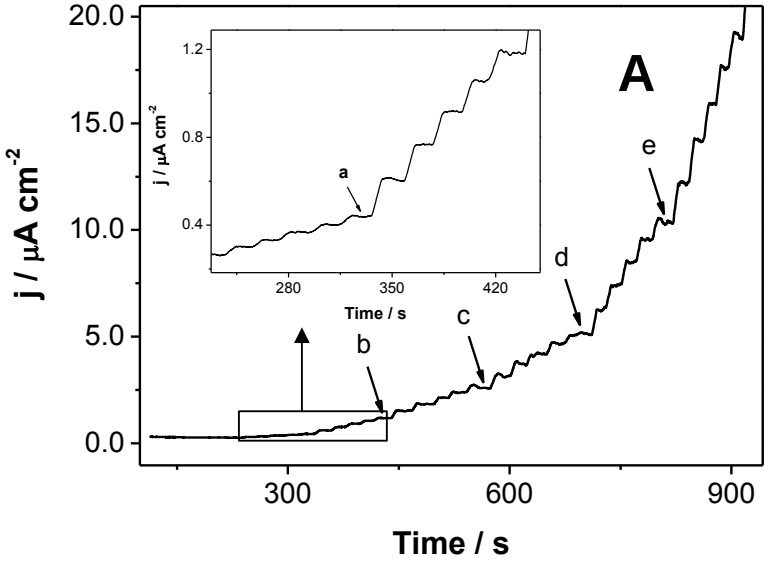

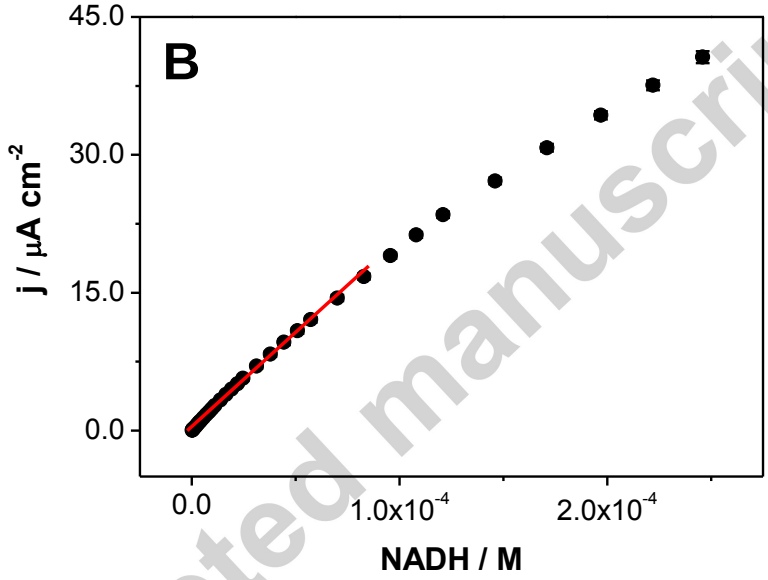

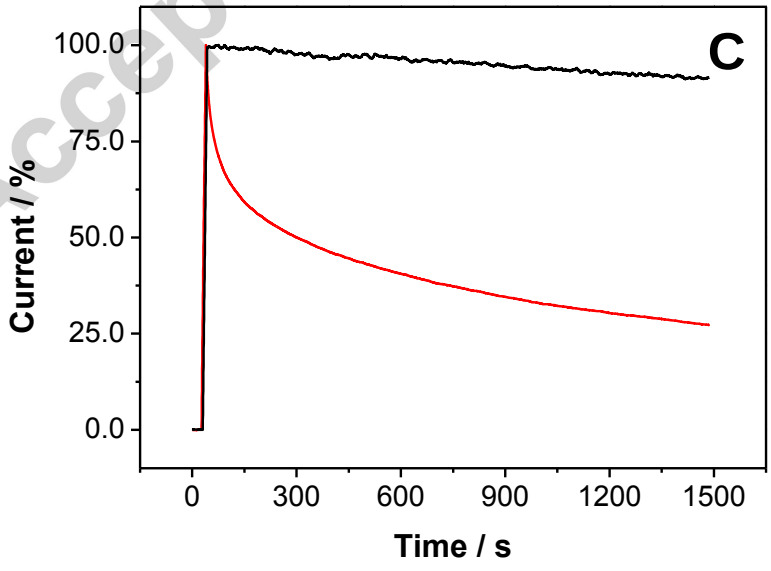

FIGURE 4- RIVAS ET AL.

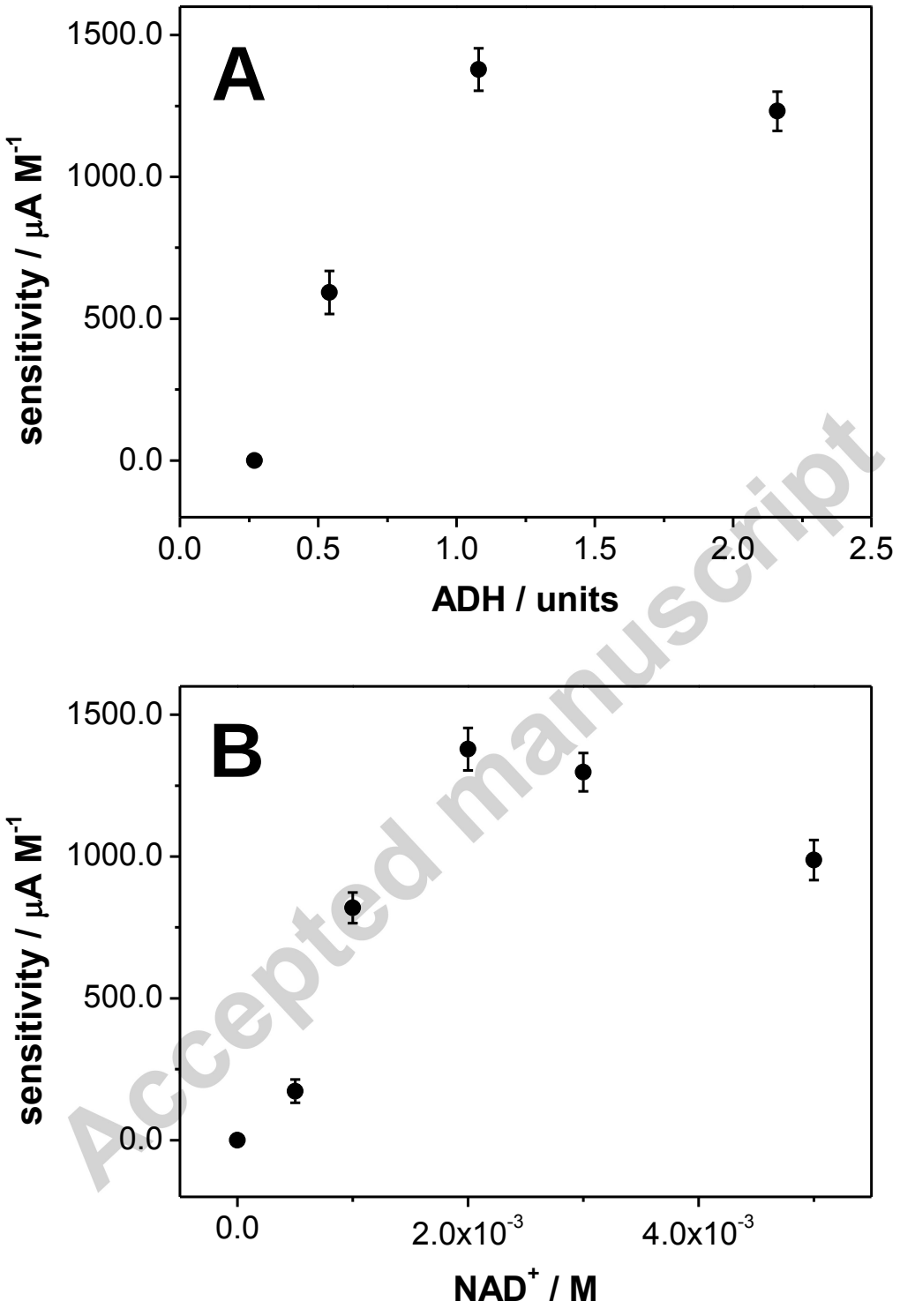

FIGURE 5- RIVAS ET AL.